

# Femtosecond micromachining in transparent bulk materials using an anamorphic lens

G. Logan DesAutels<sup>1</sup>, Chris D. Brewer<sup>2</sup>, Mark A. Walker<sup>4</sup>, Shane B. Juhl<sup>2</sup>, Marc A. Finet<sup>1</sup>, Peter E. Powers<sup>3</sup>

<sup>1</sup>AT&T Government Solutions, Dayton, OH 45433

<sup>2</sup>Air Force Research Laboratory, Materials and Manufacturing Directorate, WPAFB, OH 45433

<sup>3</sup>University of Dayton, Dayton, OH 45469

<sup>4</sup>General Dynamics Information Technology, Dayton, OH 45431

[george.desautels@wpafb.af.mil](mailto:george.desautels@wpafb.af.mil)

**Abstract:** A unique anamorphic lens design was applied to a circular 780nm femtosecond laser pulse to transform it into an elliptically shaped beam at focus. This lens was developed to give an alternative method of micromachining bulk transparent materials. The challenge for femtosecond laser processing is to control the nonlinear affect of self-focusing, which can occur when using a fast f-number lens. Once the focused spot is dominated by self-focusing the predicted focused beam becomes a filament inside the bulk, which is an undesirable effect. The anamorphic lens resolves this self-focusing by increasing the numerical aperture (NA) and employing an elliptical beam shape. The anamorphic lens was designed to furnish a 2.5 $\mu$ m by 190 $\mu$ m line at focus. Provided the pulse energy is high enough, transparent bulk material will be damaged with a single femtosecond laser pulse. Damage in this text refers to visual change in the index of refraction as observed under an optical microscope. Using this elliptical shape (or line), grating structures were micro-machined on the surface of SiC bulk transparent substrate. SiC was chosen because it is known for its micromachining difficulty and its crystalline structure. From the lack of self-focusing and using energy that is just above the damage threshold the focused line beam generated from the anamorphic lens grating structures produced a line shape nearly identical to the geometrical approximation. In this paper we discuss a new method of writing gratings (or other types of structures) in bulk transparent materials using a single femtosecond laser pulse. We will investigate the grating structures visually (inspected under an optical microscope) and also by use of an atomic force microscopy (AFM). In addition, we test the grating diffraction efficiency (DE) as a function of grating spacing,  $d$ .

© 2007 Optical Society of America

**OCIS Codes:** (220.2740) Geometric optical design; (050.2770) Gratings

---

## References and Links

1. G. Petite, P. Daguzan, S. Guizard, P. Martin, "Femtosecond History of Free Carriers in the Conduction Band of a Wide-Bandgap Oxide", Service de Recherche sur les Surfaces et l'Irradiation de la Matiere, **Bat. 462**, CE Saclay, 91191, Gif-sur-Yvette CEDEX, France.
2. A. Tien, S. Backus, H. Kapteyn, M. Murnane, G. Mourou, "Short-Pulse Laser Damage in Transparent Materials as a Function of Pulse Duration," *Phys. Rev. Lett.* **82**, 3883 (1999).
3. J. Copper, Purdue Wide Band Gap Semiconductor Device Research Program, <http://www.ecn.purdue.edu/WBG/Index.html>, Purdue University College of Engineering (2004).
4. Y. Dong, P. Molian, "Femtosecond Pulsed Laser Ablation of 3C-SiC Thin Film on Silicon," *Appl. Phys. A* **77**, 839-846 (2003).
5. J. Ashcom, C. Schaffer, E. Mazur, "Numerical Aperture Dependence of Damage and White Light Generation from Femtosecond Laser Pulses in Bulk Fused Silica," *J. Opt. Soc. Am. B* **23**, 2317-2322 (2006).

6. J. Verdeyen, "Laser Electronics," Third Edition, Prentice Hall, Inc. 1995.
7. K. Zagorulko, P. Kryukov, Y. Larionov, A. Rybaltovsky, E. Dianov, S. Chekalin, Y. Matveets, and V. Kompanets, "Fabrication of fiber Bragg gratings with 267 nm femtosecond radiation," Opt. Express **12**, 5996-6001 (2004)

## 1. Introduction

Femtosecond (fs) lasers have become an important tool for micromachining and fabrication of photonic devices. Their unique ability to induce permanent index changes into just about any transparent material arises from fast focusing conditions, resulting in very high intensities that cause nonlinear multi-photon absorption. Former research has theorized that the ultra-fast pulse interacts at the atomic electronic level [1]. It is also theorized that the fs pulse displaces electrons permanently and/or causes lattice changes resulting in a modification to the index of refraction [2]. The modification to the index is localized to a small volume depending on the NA and energy used. These index alterations can be on the surface or in most cases subsurface in bulk material.

SiC is an attractive alternative material for a variety of semiconductor devices where silicon (Si) lacks the environmental resistance that carbon furnishes when combined to Si [3]. These areas where SiC devices can be used include high-power high-voltage switching applications, high temperature electronics, and avionics where it is desired to keep sensitive Si-based electronics away from extreme environments onboard aircraft [3]. SiC is also resistant to wet chemical etching and alternative methods to bulk micromachining this material include deep reactive ion etching (DRIE) and the most direct means to micromachining SiC is reactive ion etching (RIE). These methods of processing SiC have issues related to masking or micro-masking for etching purposes, low etching rates, and an increase of processing steps [4]. The SiC sample tested is a semi-insulating type and its characteristics are shown in Table 1 below. The sample in Table 1 was perpendicularly oriented on the c-plane with the vertically polarized anamorphic beam.

Table 1. SiC sample characteristics for the semi-insulating type. These values come from the vendor, Intrinsic Corp.

Sample	Orientation	Dopant	Dopant Concentration (cm <sup>-3</sup> )	Resistivity (Ω·cm)	Thickness (μm)	Face
SiC semi-insulating	c-Plane, 6H 0° on axis	Undoped	~1x10 <sup>15</sup>	3x10	340	Si

Our method of manufacturing gratings into any transparent material can be done on or below the surface; as shown in Fig. 4. Other methods of micromachining gratings (such as fiber Bragg gratings) involve complicated methods using doped substrates and interference techniques that limit the types and size of the grating structures. Using an elliptical beam to micro-machine gratings is an alternative to interference techniques and/or circular spot direct writing using high speed translation of the sample. It provides accurate micro-machined gratings in the absence of any self-focusing from the use of a highly elliptical beam [5]. The absence of self-focusing can provide an attractive solution for ultra-fast laser applications such as free-space propagation using a collimated elliptical beam or ultra-fast propagation in transparent bulk materials. An elliptical beam has a much higher damage threshold than that of symmetrically round beams due to the lack of self-focusing in the substrate [5]. In our experiments, the numerical aperture is very large in one axis, which results in a lower damage threshold for femtosecond radiation. Here, a large NA in combination with an elliptical beam will resist the chances of any self-focusing occurring within the bulk of the sample. Self-focusing filamentation will spoil the micro-machined features, which will result in unpredictable/undesired micro-machined features. The gratings produced with the elliptical

beam generated with anamorphic lens, however, results in “clean” accurate gratings that closely resemble the geometrical profile.

## 2. Anamorphic lens design

The design and analysis of this anamorphic lens design was accomplished using the software package, Zemax. The lens system consists of two cylindrical lenses (one for x-dimension and the other for the y-dimension) and a spherical lens. The spherical lens primarily assisted the x and y cylindrical lenses to give faster foci. The lens is simple to assemble and align with the help of Thorlabs, Inc. lens tubes and standard off-shelf lenses. The lens prescription for this anamorphic lens can be provided by simply contacting the first author. The beam input into the anamorphic lens is completely characterized with pulse width,  $M^2$ , and profile measurements. The  $M^2$  refers is a measured quantity that is used to characterize the deviation from diffraction limited focusing ( $M^2$  of 1 represents the diffraction limit, and real beams have  $M^2 > 1$ ). The anamorphic lens was then characterized by measuring the numerical aperture (NA) in both axes, x and y. Figure 1 below shows a solid layout and a ray distribution through focus of the anamorphic lens.

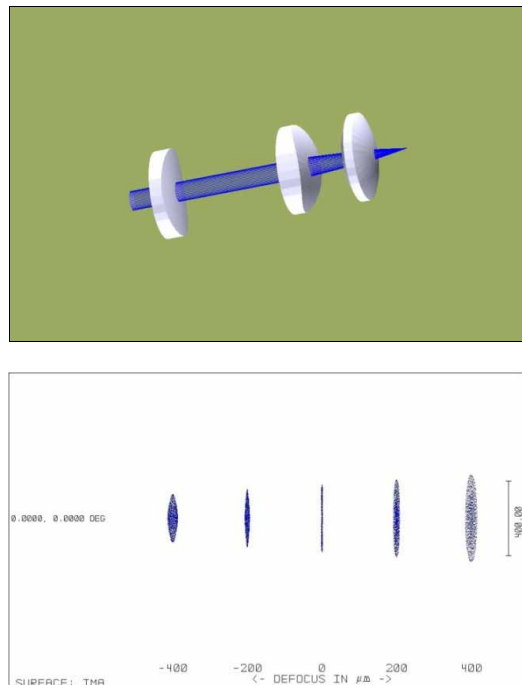


Fig. 1. Zemax analytic views of the anamorphic lens used spread the focused beam elliptically. Top is a Zemax solid layout displaying each lens and their relative position in the lens tube (on the left is a 100mm focal in x, middle is a 50mm in y, and on the right is the spherical lens), and Bottom is a plot of the ray distribution through focus  $\pm 400\mu\text{m}$ , where at defocus =  $0\mu\text{m}$  is the anamorphic line shape used for laser processing.

The lens system was designed to transform the circular beam into a line distribution as shown in Fig. 1. The x-dimension uses a 100mm focal length cylindrical lens and the y-dimension uses a 50mm focal length cylindrical lens. The last lens is a 25mm spherical lens, which is used to further assist the x and y foci into a slightly tighter focus and provide a line spread of high enough fluence above the damage threshold (DT) of the SiC substrate. Damage in this context refers to substrate modification observed under an optical microscope. The numerical aperture (NA), as mentioned, was used to characterize the anamorphic lens. A general NA equation is given below [6].

$$NA = \frac{D}{2f} = n \sin(\theta), \quad (1)$$

where D is the entrance aperture diameter, f is the effective focal length (EFL) of each axis, n, is the index of refraction, and  $\theta$  is the cone angle. The NA of this anamorphic lens system was found geometrically using Zemax and confirmed experimentally by performing a  $M^2$  measurement to extract the NA from the cone angle or slope of the data.

Figure 2 illustrates the comparative NA results between geometrical and theoretical  $M^2$  data. The NA was determined for each axis by finding the slope of a series of points after the focus. Table 2 gives both experimental and theoretical NA results of the anamorphic lens. The experimental and theoretical NA results show that the anamorphic lens design is functioning as predicted. The anamorphic lens results are compared with a commonly used spherical lens as shown in the table.

Table 2. NA values for theoretical and experimental results.

<b>Type</b>	<b>NA<sub>x</sub></b>	<b>NA<sub>y</sub></b>
Theoretical	0.073	0.131
Experimental	0.073	0.134
Instantaneous NA (at focus)	0.0035	0.256
Spherical 125mm Lens	0.022	0.022

The instantaneous NA is the NA at the desired line focus at  $0\mu\text{m}$  defocus position in Fig. 1, whereas, the theoretical and experimental NA results are for through focus which is similar to the average NA for each axis. Thus given here is the performance of the anamorphic lens as compared to theory and the NA for a line spread of  $2.5\mu\text{m} \times 190\mu\text{m}$  on the sample.

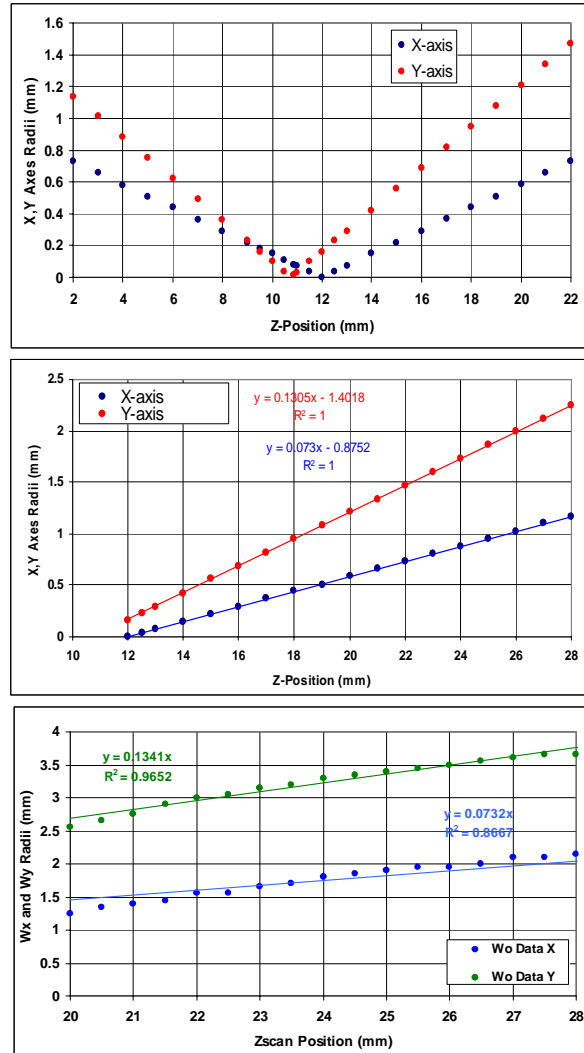


Fig. 2. Shown here is the geometrical Zemax theoretical  $M^2$  (top chart), a zoomed in theoretical chart with linear fit (middle chart), and the experimental (bottom chart), which were used to determine the NA of each axis.

### 3. Experimental setups

The anamorphic lens micromachining experiment was completed using a single laser source split to provide  $\sim 50\mu\text{J}$  to the experiment, and is shown in Fig. 3.

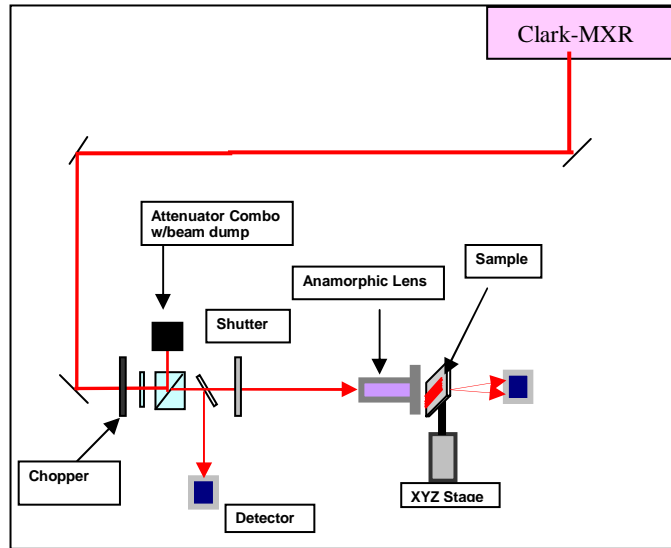


Fig. 3. Optical setup for the anamorphic lens micromachining experiment.

Figure 3 shows the experimental setup for the anamorphic lens micromachining experiment. The Clark-MXR CPA 2010 femtosecond laser system is split into multiple beam paths for different tests, and a 50 $\mu$ J portion of that is split for the experiment. The Clark laser operates using a wavelength of 780nm, a pulse width of 150-200fs,  $M^2 = 1.55$ , and a maximum energy of 1mJ per pulse at 1 kHz repetition rate. In the experimental setup there is a polarizer beam splitter and  $\frac{1}{2}$  wave plate combo used to attenuate the beam. The experiment uses the anamorphic lens to morph the 5.5mm circular beam into a 2.5 $\mu$ m x 190 $\mu$ m line distribution. Input and output photodiodes are used to measure the incident pulse energy versus the transmitted energy through the sample. Each photodiode is calibrated using a NIST traceable pyroelectric Joule meter. A chopper wheel and high speed shutter work together to automatically control the number of pulses to the sample (for this experiment a single pulse was used). Finally, the sample is held on a xyz automatic stage controlled with  $\pm 1\mu$ m accuracy. The entire illumination collection procedure is automated.

#### 4. Grating processing and characterization

Our method of micromachining gratings uses an anamorphic lens to distribute the ultrafast (UF) laser pulse from a 5.5mm round Gaussian distribution to a 2.5 $\mu$ m by 190 $\mu$ m line shape. Each individual grating line consists of three separate line pulses exposed in sequence along the x-direction and 25 lines in the vertical, equating to  $\sim 500\mu$ m x 500 $\mu$ m grating. These gratings are typically about 1 $\mu$ m to 5 $\mu$ m deep. Figure 4 shows a 500 $\mu$ m x 500 $\mu$ m grating in semi-insulating SiC with a spacing of 20 $\mu$ m.

The anamorphic line distribution processed gratings into the SiC semi-insulating sample, which were analyzed using optical microscopy and Atomic Force Microscopy (AFM) to understand the morphology of the index modified structures. The grating lines are on or just below the surface ( $\sim 5\mu$ m to 10 $\mu$ m), and the modifications deform the surface such that the machined regions protrude up from the surface. The figure below show a 10X and 50X images illustrating a good overlap of the grating lines.

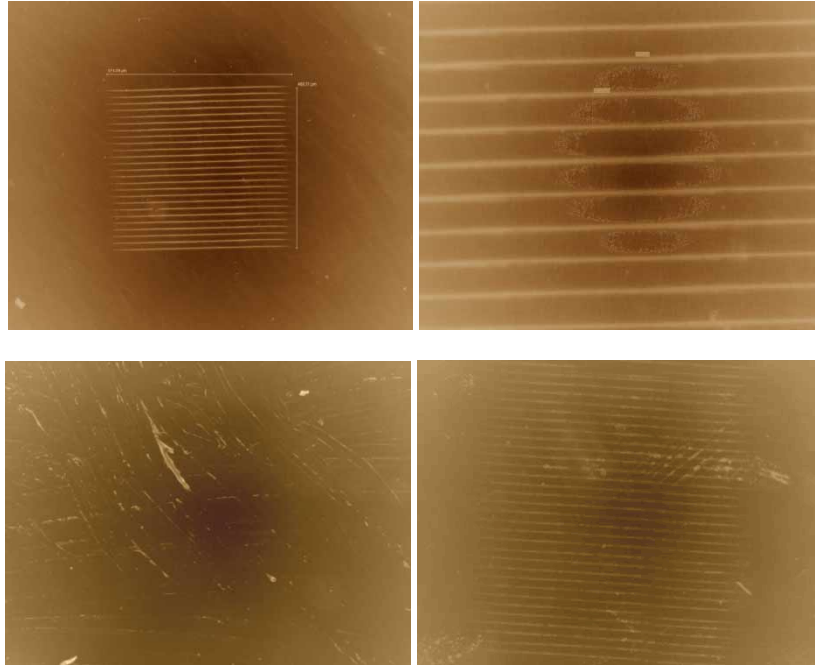


Fig. 4. (Top) SiC grating view with an optical microscope using Nomarski DIC for (left) semi-insulating SiC on a 10X magnification; (right) 50X magnification. (Bottom left) shows the surface of another SiC sample, and (bottom right) shows just 5 $\mu$ m below the surface. Image processing was performed in order to better resolve the modified surface lines.

For these images, the optical microscope used is an Olympus upright digital BX51 microscope with Nomarski DIC (Differential Interference Contrast) capabilities that use high contrast prisms to produce increased contrast/resolution. This microscope also has measuring capabilities to  $\pm 0.25\mu\text{m}$  or less, which is also NIST traceable. The optical microscope reveals that the *predicted* line spread was found experimentally to be  $\sim 4.5\mu\text{m}$  wide x  $210\mu\text{m}$  long for the semi-insulating SiC sample with a surface grating, but a  $\sim 3.5\mu\text{m}$  wide x  $190\mu\text{m}$  long grating for the subsurface grating. The processed gratings were analyzed using the Nomarski DIC mode on the optical microscope (set in reflection mode). AFM was next exercised to provide more precise imaging/measurement of the line spread morphology for the surface grating only.

The height images were obtained from monitoring the cantilever oscillation amplitude during scanning. Figure 5 below shows some AFM results of a SiC semi-insulating sample with surface line modifications.

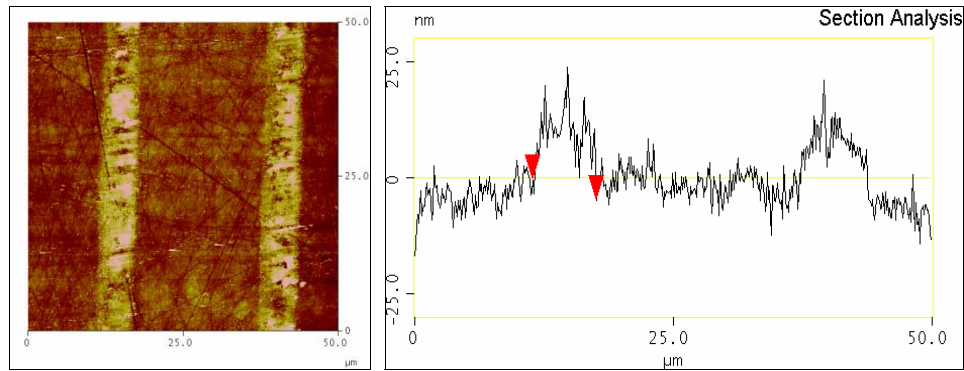


Fig. 5. AFM results of a 5.0 $\mu\text{m}$  (micron) wide and a 10nm (nano-meter) region showing a raised surface modification on semi-insulating SiC material.

The AFM morphology of the processed SiC sample is only shown for the surface grating because the subsurface topography is flat for the subsurface grating. The morphology shows a series of protruding bulges rose by  $\sim 10\text{nm}$  (nano-meters) and have a width of  $\sim 5.0\mu\text{m}$ . Upon exposure, the semi-insulating SiC surface modification by creates a hill on the substrate surface, most likely due to either local subsurface restructuring or some other electronic trapping process forcing the material to rise in the processed areas. The protruding lines caused a broader line width instead of the predicted 2.5-3.5 $\mu\text{m}$ . This trend arises from the material forced upward which causes non-irradiated areas to rise as well. If the subsurface processed lines were deeper in the bulk, this effect would be less pronounced and the processed line widths would be equal to the predicted values. This was done on a similar SiC sample, but that data is not given here.

The optimal diffraction efficiency (DE) was determined by manufacturing a series of gratings with varying spacing,  $d$ , ranging from 3 $\mu\text{m}$  to 50 $\mu\text{m}$ . A typical DE measurement output is shown in Fig. 6. This DE output in Fig. 6 shows the 0-order and diffracted beams resulting from a HeNe laser at 632.8nm, 1.5mm 1/e<sup>2</sup> beam diameter, and 1.5mW output power. A long focal length lens was used to keep the HeNe beam diameter close to 500 $\mu\text{m}$ , which is roughly the size of the grating structures. The HeNe beam power and diameter were measured with Spiricon software and a Cohu 4812 CCD camera in the absence of the gratings. The +1 and -1 orders were verified that they contained the same power within  $\pm 5\%$ . However, for the DE calculation only one of the orders were measured (the +1 order) and a factor of 2 exist in the DE calculation in Eq. (2) below.

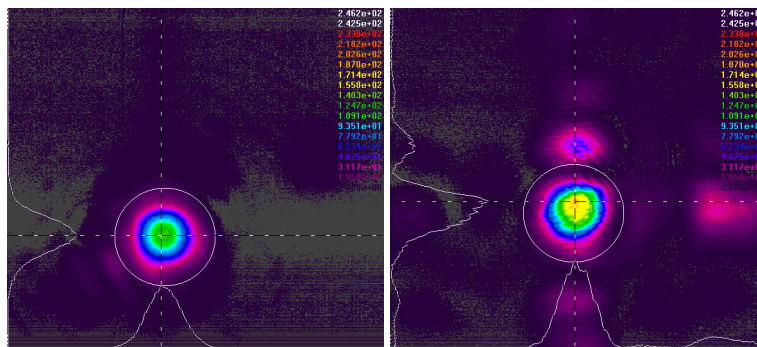


Fig. 6. This figure depicts the input 632.8nm HeNe beam and the resulting SiC diffraction pattern of the first order. On the right is the 0-order beam and on the left is the first-order diffracted beam.

Figure 6 shows on the left the 0-order beam after propagating through an unprocessed portion of the sample. There are slight higher-order diffraction rings in the 0-order image that are caused from minor surface imperfections. The 0-order beam also appears to be dimmer only because of the relative camera calibration and due to a larger ND used. On the right is the 1<sup>st</sup>-order diffraction beam, which has a structured diffraction pattern caused by the grating structure itself. Since the grating consist of three separate lines that slightly overlap, as stated earlier, this causes a superimposed diffraction pattern in the far-field (2 feet from the grating). The 1<sup>st</sup>-order appears more intense simply because of the lesser ND value used on the camera.

The DE of the 1st order diffraction pattern in Fig. 6 was calculated by first measuring the power of the 1st order then using the following equation,

$$DE = \frac{2 \cdot P_1 \cdot 10^{-(ND_0 - ND_1)}}{P_0} \cdot 100. \quad (2)$$

In Eq. (2),  $P_1$  is the power of the 1st order measured beam,  $P_0$  is the power of the zero-order beam,  $ND_0$  is the neutral density filter OD placed in front of a Cohu 4812 camera when measuring the zero-order beam (no grating present only the unprocessed sample), and  $ND_1$  is the neutral density filter OD placed in front of the Cohu camera while measuring the 1st order diffraction beam. Neutral density filters were needed to keep the CCD camera from saturating.  $P_1$  and  $P_0$  are measured using Spiricon laser beam analyzer (LBA) software with a Cohu 4812 CCD camera, which is calibrated using a Coherent FieldMax II TOP meter with an OP2-VIS detector (both traceable to NIST). Equation (2) was used to calculate the DE for each grating fabricated. Figure 7 gives the results of the DE calculated for each grating produced.

The uncertainty in the DE measurement was determined using standard propagation of uncertainties. The uncertainties are primarily from the FieldMax meter, which has  $\pm 1\%$  accuracy, and the neutral density filters ( $ND_0$  and  $ND_1$ ) that are  $\pm 4\%$ . The OP2-VIS detector has  $\pm 5\%$  calibration uncertainty, but since we are taking relative measurements (or the ratio of  $P_1$  to  $P_0$ ) the 5% can be negated since it cancels. Therefore, the overall error in Eq. (2) is taking into account the  $\pm 1\%$  for the meter accuracy and  $\pm 4\%$  for the ND values. From standard error analysis the uncertainty in DE is  $\pm 5\%$  or less.

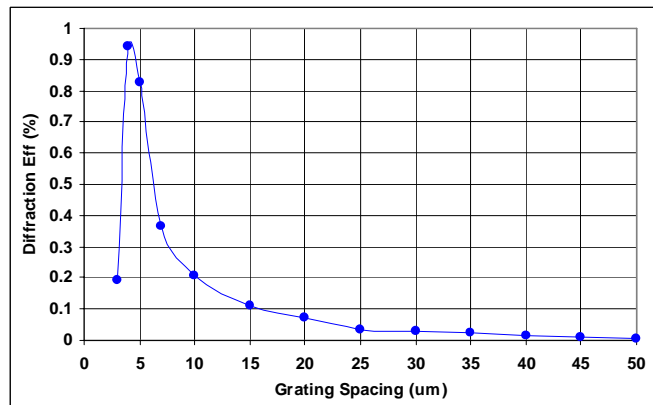


Fig. 7. DE verses grating spacing.

Figure 7 demonstrates how the DE peaks at a grating spacing of  $4\mu\text{m}$ . The DE was measured using a HeNe 632nm laser aligned nearly perpendicular ( $0^\circ$  to  $5^\circ$ ) to the micro-machined grating and to the c-axis of the SiC crystal. Once the HeNe beam passed through

the grating it was diffracted, and the 1<sup>st</sup> order diffracted beam was measured by a camera roughly 2 feet away. The diffraction angle, power, and the image of the 1<sup>st</sup> order beam for each grating were measured at the same distance of 2 feet. These DE results are primarily shown here to illustrate how the gratings generated, using this anamorphic lens technique, in SiC present a practical alternative method of constructing gratings in transparent materials.

## 5. Conclusion

In this work we report a new way of processing transparent bulk materials and grating structures using an anamorphic lens design that enables a single femtosecond pulse to modify the surface and/or subsurface with a change in the bulk index of refraction. The theoretical anamorphic lens design agrees well with the experimental characterization of  $M^2$  and NA results. The gratings manufactured are  $\sim 500\mu\text{m} \times 500\mu\text{m}$  and are easy to acquire good alignment of the individual line pulses. Optical microscopy and AFM results show the morphology of these grating lines to be in good agreement with the predicted results. However, depending on the subsurface depth and type of substrate irradiated, a protrusion will form above the surface, which causes broadening of the machined line width. The DE results illustrate the performance of the gratings fabricated in SiC, which show the gratings produced are of good quality. One functional application for this technique is manufacturing fiber Bragg gratings (FBG) [7]. This technique can generate gratings without removing the cladding, using a phase mask, or adding dopant to the fiber to react to the UV interfering beams to create the FBG. Special thanks is given to AFRL personal Dr. Don Dorsey, Mr. Tom Kensky for providing the SiC samples, to Dr. Bill Mitchell for providing information on each of the SiC samples, and to Dr. Angela Campbell for assisting with AFM results.